Inorganic Chemistry

Article

pubs.acs.org/IC

Two Compounds Constructed from Bimolybdenum-Capped Sandwich-Type Tetra-Ni-molybdogermanate and N-Donor Multidentate Ligand

Shi Zhou,[†,‡] Bo Liu,[‡] Tian Shi,[†] Xiao-Min Li,[†] and Ya-Guang Chen*[,†]

[†]Key Laboratory of Polyoxometalates Science of Ministry of Education, Faculty of Chemistry, Northeast Normal University, Changchun 130024, P. R. China

[‡]College of Chemistry, Jilin Normal University, Siping 136000, P. R. China

Supporting Information

ABSTRACT: Two organic−inorganic hybrid bimolybdenum-capped tetra-Ni^{II} sandwich-type molybdogermanates, namely, $(H_2L)_4[Ni_4(H_2O)_2\{B\text{-}\alpha\text{-}GeMo_9O_{34}(MoO_2)\}_2]\cdot 6H_2O$ (**1**), $[Ni_2(HL)_4(H_2O)_2][Ni_4(H_2O)_2\{B\text{-}\alpha\text{-}GeMo_9O_{34}(MoO_2)\}_2]\cdot 12H_2O$ (**2**), L = 2,4,5-tri(4-pyridyl)imidazole, were prepared with hydrothermal synthesis method and characterized by elemental analysis, IR spectroscopy, powder X-ray diffraction, thermogravimetric analysis, and single-crystal X-ray diffraction. Their magnetic properties and electrochemical properties were investigated. The results show that compounds **1** and **2** contain a new bimolybdenum-capped sandwich-type heteropolymolybdate anion, $[Ni_4(H_2O)_2\{B\text{-}\alpha\text{-}GeMo_9O_{34}(MoO_2)\}_2]^{8-}$. The compound **1** is a zero-dimensional supramolecular compound, and the supramolecular architecture of compound **2** is constructed from covalent layers through hydrogen bonds and $\pi-\pi$ interaction. The two compounds both present electrocatalytic activities for the reduction of nitrite.

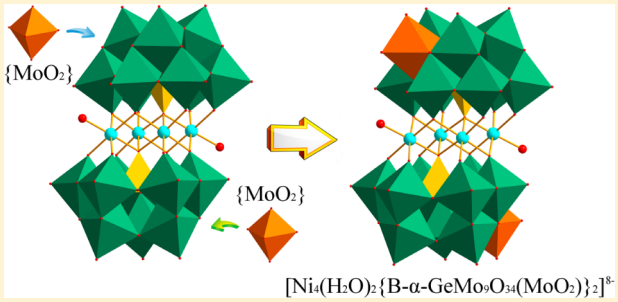

INTRODUCTION

Transition-metal-substituted polyoxometalate (TMSP) clusters constructing on traditional lacunary Keggin frameworks is a hot research point in catalysis, biopharmaceuticals, and physical fields, which is due to their potential applications in such fields. Thus, the design and synthesis of TMSP are receiving more attention recently.[1−7] The sandwich-type $[Co_4(H_2O)_2(B\text{-}\alpha\text{-}PW_9O_{34})_2]^{10-}$ was first synthesized in 1973.[8] Since then most investigations about sandwich-type TMSPs have focused on heteropolytungstates (HPTs), while few researches on sandwich-type heteropolymolybdates (HPMs) have been reported.[9−13] The reason for this is that the lacunary heteropolytungstate (L-HPT) anions are easy to control in aqueous solution, retaining the stable vacant structure; in contrast, the kinetic instability of the lacunary heteropolymolybdate (L-HPM) anions makes them hard to construct.[14] So how to achieve a reasonable synthesis of TMSP based on the L-HPM anions is very challenging for researchers.

Fukushima reported the first sandwichlike heteropolymolybdate $[Cu_2(SiMo_9O_{33})_2]^{12-}$ based on L-HPM anion of $[SiMo_9O_{33}]^{8-}$ in 1981.[15] After that, only a few studies on coordination compounds based on the L-HPM anions have been reported. The tetra-TM sandwich-type molybdogermanate $[Na_{11}(H_2O)_{25}]H[M_4(H_2O)_2(B\text{-}\alpha\text{-}GeMo_9O_{34})_2]\cdot 6H_2O$ (M = Ni; Mn; Co) based on the trivacant Keggin ion $[B\text{-}\alpha\text{-}GeMo_9O_{34}]^{10-}$ was first found by Niu et al. in 2009.[16] One year later, one-dimensional chainlike molybdogermanate $(Him)_8Na_7H_7[Cu(im)_4(CuGeMo_9O_{33})_2]$ $[(CuGeMo_9O_{33})_2]$ (im = imidazole), based on a TM sandwich-type B-β-molybdogermanate was discovered by Xu's group.[17] However, the organic sections only act as countercations in most of the tetra-TM sandwich-type TMSPs. The study on inorganic−organic complex with two-dimensional (2D) or three-dimensional (3D) structures constructed from tetra-TM sandwich-type TMSPs and N-donor multidentate ligand remain less developed. Therefore, the synthesis and exploration of sandwich-type TMSPs with high-dimensional (i.e., 2D or 3D) structure construed on the L-HPM anions and N-donor multidentate ligand are very important research frontiers in polyoxometalate chemistry.

Some studies indicated that L-HPM could be stabilized after it was capped by {V═O}, {Sb}, {As}, {AsO}, and {M-ligand} (M = Cu, Ni, Co, Ag, etc.).[18−20] In 2011, Niu's group reported three unique heteropolymolybdates building on monocapped trivacant $[As^{III}As^{V}Mo_9O_{34}]^{6-}$ fragments that derived from the infrequent trivacant Keggin $[A\text{-}\alpha\text{-}As^{V}Mo_9O_{34}]^{9-}$ fragment with a capping $\{AsO_3\}$ group.[21] Through this inspiration, we thought whether we can construct L-HPM by introducing capped groups. Through inspiration of this strategy, a sandwich-type tetra-Ni-molybdogermanate polyoxoanion $[Ni_4(H_2O)_2\{B\text{-}\alpha\text{-}GeMo_9O_{34}(MoO_2)\}_2]^{8-}$ with two capped

Received: February 3, 2015
Published: July 22, 2015

DOI: 10.1021/acs.inorgchem.5b00227
Inorg. Chem. 2015, 54, 7165−7170

{MoO_2} groups was obtained through a large number of experiments by adjusting the proportion of reactants and initial pH value. It is worth mentioning that bimolybdenum-capped sandwich-type TMSP has not been experimentally determined.

On the basis of the above point of view, we successfully incorporated a N-donor multidentate ligand with novel bimolybdenum-capped sandwich-type tetra-Ni molybdogermanates and obtained two novel bimolybdenum-capped sandwich-type TMSPs under hydrothermal conditions: $(H_2L)_4[Ni_4(H_2O)_2\{B\text{-}\alpha\text{-}GeMo_9O_{34}(MoO_2)\}_2]\cdot 6H_2O$ (**1**) and $[Ni_2(HL)_4(H_2O)_2][Ni_4(H_2O)_2\ \{B\text{-}\alpha\text{-}GeMo_9O_{34}(MoO_2)\}_2]\cdot 12H_2O$ (**2**), L = 2,4,5-tri(4-pyridyl)imidazole. Interestingly, the reaction conditions are the same for compounds **1** and **2** during the process of formation, except subtle difference of pH values. Notably, **2** not only is the first example of bimolybdenum-capped sandwich-type tetra-Ni-molybdogermanate based on N-donor multidentate ligand, but also the rare 2D inorganic−organic composite structures constructed from sandwich-type TMSPs.

EXPERIMENTAL SECTION

Materials and Methods. Organic ligand L was prepared by the general method.[22] Other reagents were purchased from commercial sources and used as received. The Fourier transform infrared (FTIR) spectra were recorded in the range of 4000−400 cm^{-1} on a Mattson Alpha-Centauri spectrometer. Elemental analyses of C, H, and N were performed on a Perkin-Elmer 2400 CHN elemental analyzer, and those of Ni and Mo were performed with a Leaman ICP spectrometer. Thermogravimetric analyses were performed on a Perkin-Elmer TGA7 instrument in N_2 atmosphere at a heating rate of 10 °C min^{-1}. The powder X-ray diffraction (PXRD) data were recorded on a Siemens D5005 diffractometer with Cu Kα (λ = 1.5418 Å) radiation. Variable-temperature direct current magnetic susceptibility measurements were performed on the polycrystalline samples in an applied magnetic field of 1000 Oe over the temperature range of 2.0−300 K using a Quantum Design XL-5 SQUID magnetometer. Electrochemical measurements were performed at room temperature on CHI 660C electrochemical workstation.

Syntheses. *$(H_2L)_4[Ni_4(H_2O)_2\{B\text{-}\alpha\text{-}GeMo_9O_{34}(MoO_2)\}_2]\cdot 6H_2O$ (**1**).* L (0.03 g, 0.1 mmol), $Ni(CH_3COO)_2\cdot 4H_2O$ (0.05 g, 0.2 mmol), GeO_2 (0.01g, 0.1 mmol), $Na_2MoO_4\cdot 2H_2O$ (0.242g, 1 mmol), and water (10 mL) were mixed and placed in a Teflon reactor (18 mL), which was heated at 170 °C for 5 d. The initial pH value of the mixture was ∼4.5. The reactor was cooled to room temperature at a rate of 10 °C·h^{-1}, and yellow crystals of **1** were collected in 37% yield based on L. The final pH value was ∼4.2. Anal. Calcd for $C_{36}H_{38}GeMo_{10}N_{10}Ni_2O_{40}$ (M_r = 2400.17): C, 18.02; H, 1.6; N, 5.84; Ni, 4.89; Mo, 39.97. Found: C, 17.93; H, 1.54; N, 5.78; Ni, 4.98; Mo, 39.78%. FTIR (KBr pellet, cm^{-1}): 3460(s), 1629(s), 1510(m), 1487(w), 1201(m), 1128(w), 1065(w), 934(s), 882(s), 805(m), 778(s), 712(m), 487(m).

*$[Ni_2(HL)_4(H_2O)_2][Ni_4(H_2O)_2\{B\text{-}\alpha\text{-}GeMo_9O_{34}(MoO_2)\}_2]\cdot 12H_2O$ (**2**).* L (0.03 g, 0.1 mmol), $Ni(CH_3COO)_2\cdot 4H_2O$ (0.05 g, 0.2 mmol), GeO_2(0.01 g, 0.1 mmol), $Na_2MoO_4\cdot 2H_2O$ (0.242 g, 1 mmol), and water (10 mL) were mixed and placed in a Teflon reactor (18 mL). The reator was heated at 170 °C for 5 d. The initial pH value of the mixture was ∼4.8. The reactor was cooled to room temperature at a rate of 10 °C·h^{-1}, and green crystals of **2** were collected in 21% yield based on L. The final pH value was ∼4.3. Anal. Calcd for $C_{36}H_{44}GeMo_{10}N_{10}Ni_3O_{44}$ (M_r = 2528.93): C, 17.10; H, 1.75; N, 5.54; Ni, 6.96; Mo, 37.94. Found: C, 17.13; H, 1.70; N, 5.43; Ni, 6.84; Mo, 37.67%. FTIR (KBr pellet, cm^{-1}): 3436(s), 1615(s), 1486(w), 1429(w), 1384(s), 1253(m), 1198(m), 935(s), 878(s), 780(s), 715(m), 498(w).

X-ray Crystallography. The X-ray diffraction data of compounds **1** and **2** were collected on a Bruker Smart Apex II diffractometer with graphite monochromatic Mo Kα radiation (λ = 0.710 73 Å) at 293 K with ω scans. Multiscan absorption corrections were applied. The structures were solved by direct methods and refined by full matrix least-squares on F^2 using the SHELXTL crystallographic software package.[23] The positions of hydrogen atoms on the carbon atoms were calculated theoretically, and the hydrogen atoms on N1, N5, N6, and N9 were found in a difference map.

RESULTS AND DISCUSSION

Crystal Structure Description. Structural analyses indicate that the compounds **1** and **2** all contain a novel bimolybdenum-capped sandwich-type tetra-Ni-molybdogermanate polyoxoanion $[Ni_4(H_2O)_2\{B\text{-}\alpha\text{-}GeMo_9O_{34}(MoO_2)\}_2]^{8-}$. A unique modified Weakley-type sandwichlike molybdogermanate derivative $[Ni_4(H_2O)_2\{B\text{-}\alpha\text{-}GeMo_9O_{34}(MoO_2)\}_2]^{8-}$ was synthesized, through capping the sandwich-type molybdogermanate polyoxoanion $[Ni_4(H_2O)_2(B\text{-}\alpha\text{-}GeMo_9O_{34})_2]^{12-}$ with two {MoO_2} subunits on its two oppositely disposed tetragonal faces (Figure 1). The structural unit, $[Ni_4(H_2O)_2\{B\text{-}\alpha\text{-}GeMo_9O_{34}(MoO_2)\}_2]^{8-}$, consists of two $[B\text{-}\alpha\text{-}GeMo_9O_{34}]^{10-}$ anions capped by a {MoO_2} group and a rhomblike Ni_4O_{16} group. The Ni_4O_{16} unit is constructed via four edge-shared NiO_6 octahedra as in other reported M_4O_{16} of Weakley-type sandwich polyoxometalates.[8,16] The NiO_6 octahedra are highly distorted with Ni−O distances Ni1−O of 2.019(5)−2.082(5) Å (average (av) 2.059 Å) and Ni2−O of 2.024(5)−2.114(5) Å (av 2.066 Å). The diagonal Ni···Ni separations in the Ni_4O_{16} group are 5.305 Å for Ni1···Ni1 and 3.141 Å for Ni2···Ni2, and the distances of the two adjacent Ni atoms in rhomblike Ni_4O_{16} clusters are 3.084 and 3.082 Å. In B-α-$GeMo_9O_{34}$ unit there are three different types of Mo−O bonds: 1.744(5)−2.203 (5) Å for Mo−O_b (O_b = bridging oxygen), 1.684(5)−1.708 (5) Å for Mo−O_t (O_t = terminal oxygen) of the MoO_6 unit, and 2.256(4)−2.388 (5) Å for Mo−O_c (O_c = central oxygen of Mo−O−Ge). The parent core displays a classical Weakley-type sandwich polyoxoanion skeleton. In the two capping {MoO_2} subunits, the distances between Mo−O bonds are within a narrower range compared with normal ones: the range for two short Mo−O_t bonds is from 1.703(5) to 1.706 (5) Å, while the one for four longer Mo−O_b bridging bonds is from 2.000(5) to 2.209(5) Å. Many factors influenced the successful synthesis of the anionic cluster, such as the temperature, metal ions, pH value, and nature of the counteraction. The reaction temperature and Ni^{2+} ion are vital during synthesizing process. When the temperature and the kind of metal ions were changed, the crystalline sample could not be obtained. The formation of $[Ni_4(H_2O)_2\{B\text{-}\alpha\text{-}GeMo_9O_{34}(MoO_2)\}_2]^{8-}$ could also be influenced by the solution pH values. The mechanism is, possibly, such that when we set the pH range to 4.5−5.0, the formation of $[Ni_4(H_2O)_2(B\text{-}\alpha\text{-}GeMo_9O_{34})_2]^{12-}$ is favored. Since the $[Ni_4(H_2O)_2(B\text{-}\alpha\text{-}GeMo_9O_{34})_2]^{12-}$ has higher negative charge,

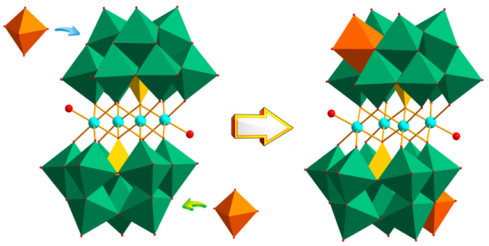

Figure 1. Polyhedral representation of $[Ni_4(H_2O)_2\{B\text{-}\alpha\text{-}GeMo_9O_{34}(MoO_2)\}_2]^{8-}$ where the orange polyhedral corresponds to the {MoO_2} unit.

DOI: 10.1021/acs.inorgchem.5b00227
Inorg. Chem. 2015, 54, 7165−7170

the remaining Mo(VI) (the molar ratio of Ge/Mo in starting materials is 1:10) in the form of $\{MoO_2^{2+}\}$ unit is added to reduce the negative charge and give the most stable product.[24]

By comparison with the first tetra-TM sandwich-type HPMs $[M_4(H_2O)_2(B\text{-}\alpha\text{-}GeMo_9O_{34})_2]^{12-}$ molybdogermanate anion,[16] we found that the first tetra-TM sandwich-type HPM $[M_4(H_2O)_2(B\text{-}\alpha\text{-}GeMo_9O_{34})_2]^{12-}$ was synthesized by a routine method, while the $[Ni_4(H_2O)_2\{B\text{-}\alpha\text{-}GeMo_9O_{34}(MoO_2)\}_2]^{8-}$ was formed by hydrothermal method. We utilized simple raw materials instead of trivacant HPM precursors, and the pH range was from 4.5 to 5.0 in synthesizing the two kinds of polyanions. The structure of the two kinds of anions are the same except two more $\{MoO_2\}$ subunits are on the $[Ni_4(H_2O)_2\{B\text{-}\alpha\text{-}GeMo_9O_{34}(MoO_2)\}_2]^{8-}$ than on the $[M_4(H_2O)_2(B\text{-}\alpha\text{-}GeMo_9O_{34})_2]^{12-}$.

Structure of $(H_2L)_4[Ni_4(H_2O)_2\{B\text{-}\alpha\text{-}GeMo_9O_{34}(MoO_2)\}_2]\cdot 6H_2O$ (1). The asymmetric unit of **1** is made of two L ligands, half of one $[Ni_4(H_2O)_2\{B\text{-}\alpha\text{-}GeMo_9O_{34}(MoO_2)\}_2]^{8-}$, and three lattice water molecules (Supporting Information Figure S1). The protonated L ligands with parallel arrangement in compound **1** play the role of the counterions to counteract the charges of polyoxoanion. Stronger $\pi-\pi$ interactions are likely to occur between L ligands with C−C/N distances of 3.340−3.595 Å. Hydrogen-bonding interaction between molecular units is within the typical hydrogen bond distances (Supporting Information Table S3), which contributes to stabilizing the crystal structure and forming 3D supramolecular structure (Figure 2).

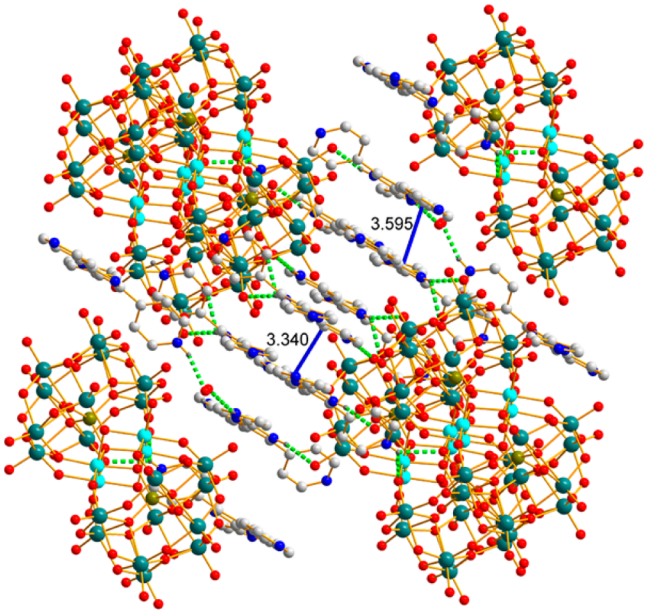

Figure 2. 3D supramolecular structure stabilized by hydrogen bonding and $\pi-\pi$ interaction. Blue bar shows the $\pi-\pi$ interaction and green dot line, hydrogen bonds.

Structure of $[Ni_2(HL)_4(H_2O)_2][Ni_4(H_2O)_2\{B\text{-}\alpha\text{-}GeMo_9O_{34}(MoO_2)\}_2]\cdot 12H_2O$ (2). There are one Ni^{2+} ion, two protonated L ligands, half of one $[Ni_4(H_2O)_2\{B\text{-}\alpha\text{-}GeMo_9O_{34}(MoO_2)\}_2]^{8-}$, one coordinated water molecule, and six lattice water molecules in the asymmetric unit of compound **2** (Supporting Information Figure S2). The Ni^{2+} ion is coordinated by four pyridyl nitrogen atoms from four different L ligands, one terminal oxygen atom from $[Ni_4(H_2O)_2\{B\text{-}\alpha\text{-}GeMo_9O_{34}(MoO_2)\}_2]^{8-}$ anion, and one water molecule, exhibiting a distorted octahedral coordination geometry. Ligand L acts as a bidentate ligand connecting two Ni^{2+} ions forming NiL_2 chain with a 46-membered ring and 22-membered ring extending along crystallographic *a*-axis (Figure 3); in turn,

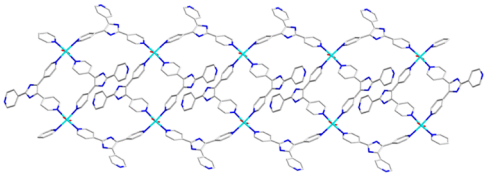

Figure 3. NiL_2 chain with a 46-membered ring and 22-membered ring.

$[Ni_4(H_2O)_2\{B\text{-}\alpha\text{-}GeMo_9O_{34}(MoO_2)\}_2]^{8-}$ anion acts as a bidentate ligand connecting two Ni^{2+} ions of two chains forming a 2D layer structure (Figure 4). The adjacent layers are

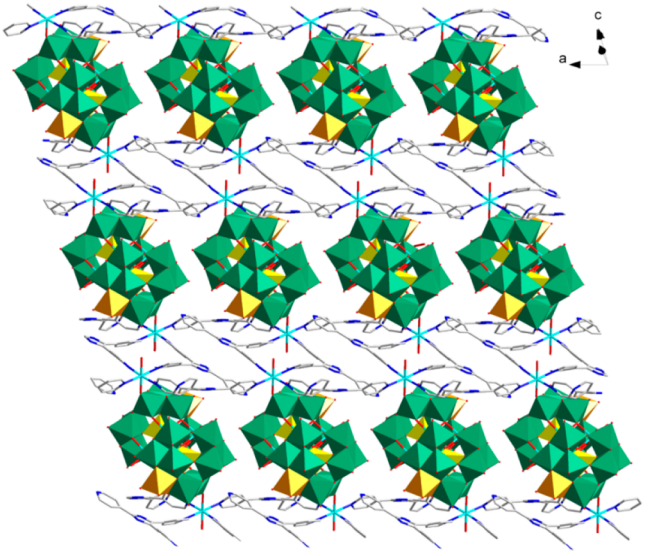

Figure 4. Ball−stick-polyhedron views of the layer structure of **2**. Hydrogen atoms and lattice water molecules are omitted for clarity.

connected by multiple intermolecular hydrogen bonds between the anions, water molecules, and L ligands, generating a 3D supermolecular network (Figure 5). Additional crystallographic details regarding compounds **1** and **2** are available in Table 1 and in the Supporting Information.

Characterization. The PXRD data for **1** and **2** were recorded and are displayed in Figures S3 and S4 (Supporting Information). The diffraction peaks of the simulated and the experimental structures match well, indicating the phase purities of these two compounds.

Thermal Analyses. The compounds **1** and **2** were thermogravimetrically analyzed to fully characterize thermal stability of the compounds. The experiment was performed in temperature range of 25−1000 °C. As presented in Supporting Information Figure S7, compound **1** lost its lattice water molecules from 120 to 170 °C (obsd. 2.4%, calcd. 2.2%). During 331−368 °C, the weight loss is due to the release of coordinated water molecules (obsd. 0.8%, calcd. 0.7%). After that temperature, the organic ligand and $[Ni_4(H_2O)_2\{B\text{-}\alpha\text{-}GeMo_9O_{34}(MoO_2)\}_2]^{8-}$ anion start to decompose from 369 to 668 °C. The residue (70%) corresponds to the formation of NiO, GeO_2, and MoO_3 (calcd. 70.3%). For **2** (Supporting

DOI: 10.1021/acs.inorgchem.5b00227
Inorg. Chem. 2015, 54, 7165−7170

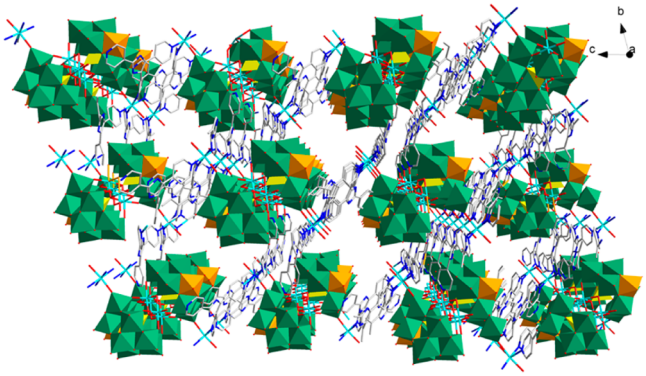

Figure 5. Combined polyhedral-ball−stick view of the 3D supramolecular network of **2**. Hydrogen atoms and lattice water molecules are omitted for clarity.

Table 1. Crystal Data and Structure Refinements of Compounds 1 and 2

	1	2
formula	$C_{36}H_{38}GeMo_{10}N_{10}Ni_2O_{40}$	$C_{36}H_{44}GeMo_{10}N_{10}Ni_3O_{44}$
FW	2400.17	2528.93
crystal system	triclinic	triclinic
space group	$P\bar{1}$	$P\bar{1}$
a/Å	13.2203(6)	13.105(5)
b/Å	15.6458(7)	15.255(5)
c/Å	16.3157(8)	19.002(5)
α (deg)	70.8320(10)	71.970(5)
β (deg)	69.5920(10)	74.560(5)
γ (deg)	74.8240(10)	79.579(5)
V, Å^3	2946.0(2)	3462(2)
Z	2	2
Dc/g cm^{-3}	2.716	2.426
F(000)	2304	2436
R(int)	0.0227	0.0154
GOF on F^2	1.008	1.025
$R_1[\ I > 2\sigma(I)]$	0.0405	0.0373
ωR_2(all data)	0.1071	0.1151

Information Figure S8), the weight loss of 5.2% from 110 to 150 °C originates from the loss of its lattice water molecules (calcd. 4.3%). No further weight loss can be seen from 150 to 345 °C. After that the coordinated water molecules and organic components start to decompose from 345 to 700 °C. The residue (69.6%) corresponds to the formation of NiO, GeO_2, and MoO_3 (calcd. 69.9%).

Magnetic Properties. The magnetic properties of **1** and **2** were examined over 2−300 K and are shown in Figures 6 and 7 in the forms of χ_mT product and χ_m^{-1} versus T plots. As temperatures decreased, the χ_mT product of **1** increased from 6.485 emu K mol^{-1} at 300 K to a maximum of 14.106 emu K mol^{-1} at 14 K. This fact indicates that there exist ferromagnetic interactions between the Ni^{2+} ions of Ni4 cluster similar to those reported in refs 25−27. At the temperatures lower than 14 K, the rapid drop of the χ_mT products may be assigned to zero-field splitting (ZFS) and/or intermolecular antiferromagnetic interactions. The experimental χ_mT value of **1** at 300 K is larger than that calculated for four isolated Ni^{2+} ions (assuming S = 1, g = 2.0), which is attributed to the spinning-orbit interaction and ferromagnetic coupling. The temperature dependence of the reciprocal susceptibilities ($1/\chi_m$) in the range of 75−300 K obeys the Curie−Weiss law with C = 6.006

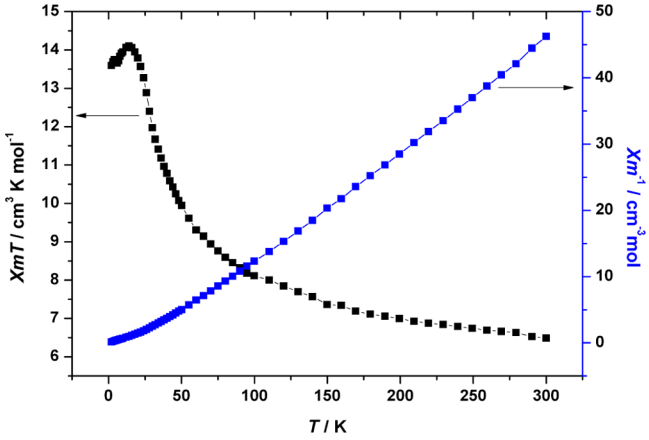

Figure 6. χ_mT product and χ_m^{-1} vs T plots of **1**.

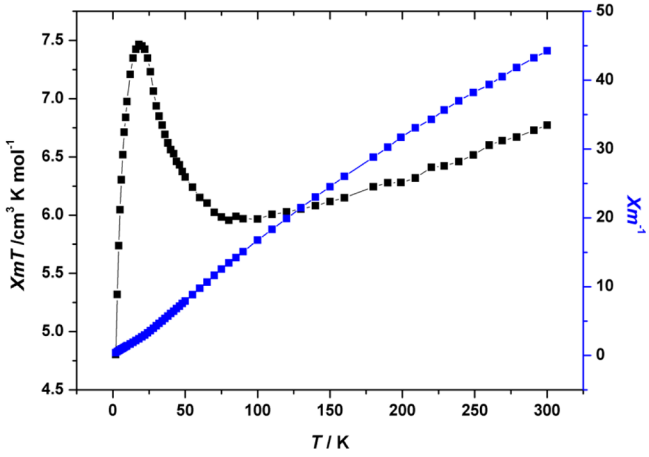

Figure 7. χ_mT product and χ_m^{-1} vs T plots of **2**.

emu K mol^{-1} and θ = 26.66 K (Supporting Information Figure S9), supporting the presence of overall ferromagnetic coupling between the Ni^{2+} ions. As supposed in other works,[28−30] the ferromagnetic coupling between the Ni^{2+} ions is exclusively transmitted through the oxo bridges due to the Ni−O−Ni angles in the range of 90−100°, where the Ni−Ni ferromagnetic exchange pathways are dominant (90 ± 14°).

The χ_mT products of **2** decreased first from 6.77 emu K mol^{-1} at 300 K to 5.95 at 80 K and then increased to a maximum of 7.47 emu K mol^{-1} at 18 K as the temperature decreased. The magnetic behavior of compound **2** in the low-temperature range (2−80 K) is similar to that of **1**, indicating the presence of ferromagnetic interactions between the Ni^{2+} ions of Ni_4O_{16} cluster. In **2** the other two Ni^{2+} ions are in the coordination polymeric chain, and the Ni atoms are separated by 10 and 11 other atoms, respectively, with Ni−Ni distances of 10.2065 and 13.1051 Å. Between the Ni^{2+} ions in the chain and that in the Ni_4 cluster are O−Mo−O atoms. Therefore, it can be supposed that the difference between **1** and **2** in the magnetic behavior results from the magnetic exchange interaction between two Ni^{2+} ions of the chain and that in the Ni_4O_{16} cluster although the bonds O−Mo−O are not considered as a good magnetic-exchange bridge. At the temperatures lower than 18 K, the rapid drop of the χ_mT products may also be assigned to ZFS. The experimental χ_mT values of **2** at 300 K are larger than expected for six isolated

DOI: 10.1021/acs.inorgchem.5b00227
Inorg. Chem. 2015, 54, 7165−7170

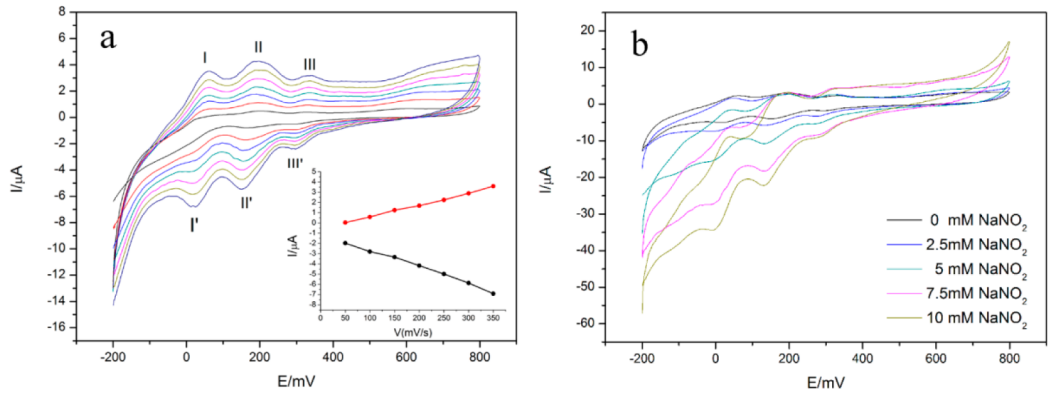

Figure 8. (a) Cyclic voltammograms of **1-CPE** in 1 mol·L^{-1} H_2SO_4 under different scan rates from inner to outer: 50, 100, 150, 200, 250, 300, and 350 mV·s^{-1}. (inset) Plots of the anodic and the cathodic peak II−II′ currents against scan rates. (b) Cyclic voltammograms of **1-CPE** in a 1 mol·L^{-1} H_2SO_4 solution containing $NaNO_2$. (upper to lower) $NaNO_2$ concentrations 0, 2.5, 5, 7.5, and 10 mM, at a scan rate of 250 mV·s^{-1}.

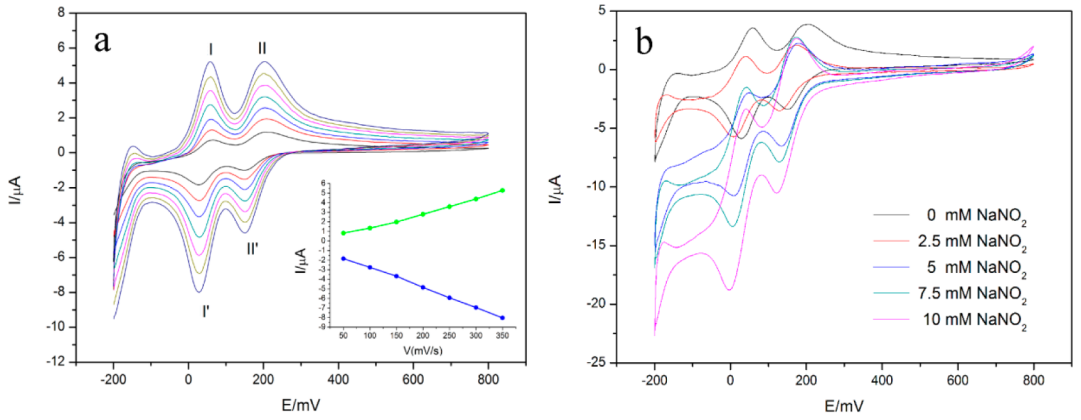

Figure 9. (a) Cyclic voltammograms of **2-CPE** in 1 mol·L^{-1} H_2SO_4 under different scan rates from inner to outer: 50, 100, 150, 200, 250, 300, and 350 mV·s^{-1}. (inset) Plots of the anodic and the cathodic peak I−I′ currents against scan rates. (b) Cyclic voltammograms of **2-CPE** in a 1 mol·L^{-1} H_2SO_4 solution containing $NaNO_2$. (upper to lower) $NaNO_2$ concentrations 0, 2.5, 5, 7.5, and 10 mM, at a scan rate of 250 mV·s^{-1}.

Ni^{2+} ions (6.40 for S = 1, g = 2.0), which is attributed to the spinning−orbit interaction and ferromagnetic coupling.

Electrochemical Characterization. We investigated the electrochemical behaviors and electrocatalytic nitrite reduction of **1**-carbon paste electrode (CPE) and **2**-CPE. The cyclic voltammograms for **1**-CPE were recorded in 1 M H_2SO_4 aqua solution with different scan rates and are displayed in Figure 8a. In the potential range from −200 to +800 mV, there are three pairs of reversible redox peaks I−I′, II−II′, and III−III′; their mean peak potentials $E_{1/2} = (E_{pc} + E_{pa})/2$ are 41, 174, and 315 mV (scan rate: 250 mV·s^{-1}), respectively. The three pairs of redox peaks correspond to three two-electron reduction processes of Mo. When the scan rate is raised from 50 to 350 mV·s^{-1}, the anodic peak potentials, which are positive-going, shift, while the corresponding cathodic peak potentials shifts toward the opposite direction. Their peak currents are proportional to the scan rates, indicating the redox process of **1**-CPE is surface-controlled. In the potential range from −200 to +800 mV for **2**-CPE, there are two pairs (I−I′ and II−II′) of reversible redox peaks at $E_{1/2}$= 44 and 178 mV for **2**-CPE, which should be assigned to the two consecutive one-electron redox processes of Mo (Figure 9a; scan rate: 250 mV·s^{-1}). When the scan rate was varied from 50 to 350 mV·s^{-1}, the electrochemical behavior of **2**-CPE followed the same trends as that of **1**-CPE, indicating its redox process is also surface-controlled.

The nitrite electrocatalytic reductions on **1**-CPE and **2**-CPE can be seen clearly in Figures 8b and 9b, which show cyclic voltammograms in 1 mol·L^{-1} H_2SO_4 solution under scan rate 250 mV·s^{-1}. With the increase of nitrite concentration, the peak currents of three reduction peaks tend to increase, while the ones for the oxidation peaks incline to decrease, which indicates that the reducing process of nitrite produces two-, four-, and six-electron reduced species on **1**-CPE. For **2**-CPE, the peaks currents of two reduction and oxidation peaks follow the same trends, involving two- and four-electron reduced species on **2**-CPE.

With the increase of their reduction degree, electric catalytic activity of **1**-CPE and **2**-CPE increased. Note that high scan rate (250 mV·s^{-1}) is appropriate to be used for the electrocatalytic reduction of nitrite and to obtain noticeable catalytic currents, so an obviously fast reduction of nitrite can be achieved at the **1**-CPE and **2**-CPE. Hence the two compounds may be used as potential electrocatalysts.

■ CONCLUSION

Two bimolybdenum-capped tetra-Ni^{II} sandwich-type molybdogermanates have been hydrothermally prepared. The L ligands act as the counterions in **1** or bidentate ligand in **2**, forming different frameworks. Magnetic measurement indicates the two compounds demonstrate ferromagnetic exchange interactions. Their electrochemical studies show that the two compounds

DOI: 10.1021/acs.inorgchem.5b00227
Inorg. Chem. 2015, 54, 7165−7170

display electrocatalytic activity for the reduction of nitrite. We successfully isolated **1** and **2**, which provide an extending prospect for the POM family. More choices of ligands to react with the new bimolybdenum-capped sandwich-type tetra-Ni molybdogermanate anion will be done in our further researches. Therefore, the systematic exploration of the bimolybdenum-capped sandwich-type heteropolymolybdates system is in progress.

■ ASSOCIATED CONTENT

Supporting Information

X-ray crystallographic data in CIF format for **1** and **2**, complementary drawings for crystal structures, thermogravimetric curves, IR curves, magnetic properties, selected bond lengths and angles, hydrogen bond tables, and PXRD patterns of compounds **1** and **2**. The Supporting Information is available free of charge on the ACS Publications website at DOI: 10.1021/acs.inorgchem.5b00227. CCDC 1023437 (for **1**) and 1023438 (for **2**) contain the supplementary crystallographic data for this paper. These data can be obtained free of charge from the Cambridge Crystallographic Data Centre via www.ccdc.cam.ac.uk/data_request/cif.

■ AUTHOR INFORMATION

Corresponding Author

*E-mail: chenyg146@nenu.edu.cn. Phone: 86-13844879154.

Notes

The authors declare no competing financial interest.

■ REFERENCES

(1) Pope, M. T.; Müller, A. *Polyoxometalates: From Platonic Solids to Anti Retroviral Activity;* Kluwer Academic Publishers: Dordrecht, The Netherlands, 1994.
(2) Special issue on polyoxometalates: *Chem. Rev.* **1998**, *98*, 1−390.
(3) Pope, M. T.; Müller, A. *Polyoxometalate Chemistry: From Topology via Self-Assembly to Applications;* Kluwer Academic Publishers: Dordrecht, The Netherlands, 2001.
(4) Kamata, K.; Yonehara, K.; Sumida, Y.; Yamaguchi, K.; Hikichi, S.; Mizuno, N. *Science* **2003**, *300*, 964−966.
(5) Anderson, T. M.; Neiwert, W. A.; Kirk, M. L.; Piccoli, P. M. B.; Schultz, A. J.; Koetzle, T. F.; Musaev, D. G.; Morokuma, K.; Cao, R.; Hill, C. L. *Science* **2004**, *306*, 2074−2077.
(6) Long, D. L.; Abbas, H.; Kögerler, P.; Cronin, L. *J. Am. Chem. Soc.* **2004**, *126*, 13880−13881.
(7) Fang, X. K.; Anderson, T. M.; Benelli, C.; Hill, C. L. *Chem. - Eur. J.* **2005**, *11*, 712−718.
(8) Weakly, T. J. R.; Evans, H. T.; Showell, J. S.; Tourne, G. F.; Tourne, C. M. *J. Chem. Soc., Chem. Commun.* **1973**, *4*, 139−140.
(9) Tian, A. X.; Ying, J.; Peng, J.; Sha, J. Q.; Han, Z. G.; Ma, J. F.; Su, Z. M.; Hu, N. H.; Jia, H. Q. *Inorg. Chem.* **2008**, *47*, 3274−3283.
(10) Zheng, P. Q.; Ren, Y. P.; Long, L. S.; Huang, R. B.; Zheng, L. S. *Inorg. Chem.* **2005**, *44*, 1190−1192.
(11) Kong, X. J.; Ren, Y. P.; Zheng, P. Q.; Long, Y. X.; Long, L. S.; Huang, R. B.; Zheng, L. S. *Inorg. Chem.* **2006**, *45*, 10702−10711.
(12) Ren, Y. P.; Kong, X. J.; Hu, X. Y.; Sun, M.; Long, L. S.; Huang, R. B.; Zheng, L. S. *Inorg. Chem.* **2006**, *45*, 4016−4023.
(13) Sha, J. Q.; Peng, J.; Lan, Y. Q.; Su, Z. M.; Pang, H. J.; Tian, A. X.; Zhang, P. P.; Zhu, M. *Inorg. Chem.* **2008**, *47*, 5145−5153.
(14) Li, F. Y.; Xu, L. *Dalton Trans.* **2011**, *40*, 4024−4034.
(15) Fukushima, H. F.; Kobayashi, A.; Sasaki, Y. *Acta Crystallogr., Sect. B: Struct. Crystallogr. Cryst. Chem.* **1981**, *37*, 1613−1615.
(16) Li, S. Z.; Zhao, J. W.; Ma, P. T.; Du, J.; Niu, J. Y.; Wang, J. P. *Inorg. Chem.* **2009**, *48*, 9819−9830.
(17) Zhao, L. L.; Luo, X. Z.; Xu, L.; Jiang, N.; Li, F. Y.; Li, Y. G. *Inorg. Chem. Commun.* **2010**, *13*, 554−557.
(18) Chen, Q.; Hill, C. L. *Inorg. Chem.* **1996**, *35*, 2403−2405.
(19) Shi, S. Y.; Sun, Y. H.; Chen, Y.; Xu, J. N.; Cui, X. B.; Wang, Y.; Wang, G. W.; Yang, G. D.; Xu, J. Q. *Dalton Trans.* **2010**, *39*, 1389−1394.
(20) Han, Z. G.; Wu, J. J.; Gao, Y. G.; Zhai, X. L. *Aust. J. Chem.* **2011**, *64*, 197−205.
(21) Han, Q. X.; Ma, P. T.; Zhao, J. W.; Wang, Z. L.; Yang, W. H.; Guo, P. H.; Wang, J. P.; Niu, J. Y. *Cryst. Growth Des.* **2011**, *11*, 436−444.
(22) Proskurnina, M. V.; Lozinskaya, N. A.; Tkachenko, S. E.; Zefirov, N. S. *Russ. J. Org. Chem.* **2002**, *38*, 1149−1153.
(23) Sheldrick, G. M. *SHELXS-97,* Program for Solution of Crystal Structures; University of Göttingen: Germany, 1997.
(24) Dolbecq, A.; Cadot, E.; Eisner, D.; Secheresse, F. *Inorg. Chem.* **1999**, *38*, 4217−4223.
(25) Gómez-Garcóa, C. J.; Borrós-Almenar, J. J.; Coronado, E.; Ouahab, L. *Inorg. Chem.* **1994**, *33*, 4016−4022.
(26) Clemente-Juan, J.; Coronado, M. E.; Galán-Mascarós, J. R.; Gómez-García, C. J. *Inorg. Chem.* **1999**, *38*, 55−63.
(27) Zhao, J. W.; Li, B.; Zheng, S. T.; Yang, G. Y. *Cryst. Growth Des.* **2007**, *7*, 2658−2664.
(28) Hou, Y.; Xu, L.; Cichon; Morgan, J.; Lense; Sheri; Hardcastle; Kenneth, I.; Hill; Craig, L. *Inorg. Chem.* **2010**, *49*, 4125−4132.
(29) Mbomekalle, I. M.; Keita, B.; Nierlich, M.; Kortz, U.; Berthet, P.; Nadjo, L. *Inorg. Chem.* **2003**, *42*, 5143−5152.
(30) Ginsberg, A. P.; Bertrand, J. A.; Kaplan, R. I.; Kirkwood, C. E.; Martin, R. L.; Sherwood, R. C. *Inorg. Chem.* **1971**, *10*, 240−246.

DOI: 10.1021/acs.inorgchem.5b00227
Inorg. Chem. 2015, 54, 7165−7170